

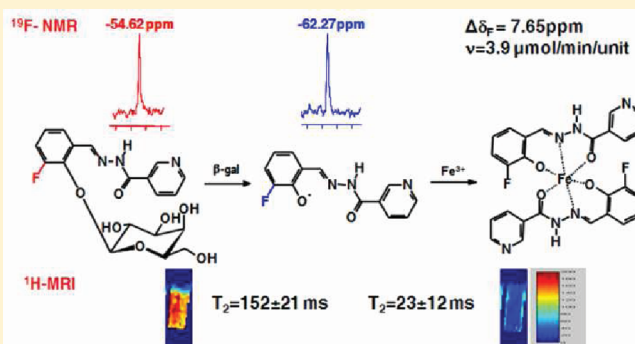
## Dual $^{19}\text{F}/^1\text{H}$ MR Gene Reporter Molecules for *in Vivo* Detection of $\beta$ -Galactosidase

 Jian-Xin Yu, Vikram D. Kodibagkar,<sup>†</sup> Rami R. Hallac, Li Liu, and Ralph P. Mason\*

Department of Radiology, The University of Texas Southwestern Medical Center, Dallas, Texas, United States

### Supporting Information

**ABSTRACT:** Increased emphasis on personalized medicine and novel therapies requires the development of noninvasive strategies for assessing biochemistry *in vivo*. The detection of enzyme activity and gene expression *in vivo* is potentially important for the characterization of diseases and gene therapy. Magnetic resonance imaging (MRI) is a particularly promising tool, since it is noninvasive and has no associated radioactivity, yet penetrates deep tissue. We now demonstrate a novel class of dual  $^1\text{H}/^{19}\text{F}$  nuclear magnetic resonance (NMR) *lacZ* gene reporter molecule to specifically reveal enzyme activity in human tumor xenografts growing in mice. We report the design, synthesis, and characterization of six novel molecules and evaluation of the most effective reporter in mice *in vivo*. Substrates show a single  $^{19}\text{F}$  NMR signal and exposure to  $\beta$ -galactosidase induces a large  $^{19}\text{F}$  NMR chemical shift response. In the presence of ferric ions, the liberated aglycone generates intense proton MRI  $T_2$  contrast. The dual modality approach allows both the detection of substrate and the imaging of product enhancing the confidence in enzyme detection.



### INTRODUCTION

Several reporter proteins have been used in gene expression and regulation studies including  $\beta$ -galactosidase ( $\beta$ -gal), firefly luciferase (*luc*),  $\beta$ -glucuronidase, fluorescent proteins (such as green fluorescent protein, GFP), transferrin and ferritin, the enzymes creatine and arginine kinase, tyrosinase, and polycations such as poly lysine.<sup>1,2</sup> Historically, the *lacZ* gene encoding  $\beta$ -gal has been widely used with applications ranging from molecular biology to small animal investigations and clinical trials including assays of clonal insertion, transcriptional activation, protein expression, and protein interaction.<sup>3,4</sup> Recently, various innovative approaches to assessing  $\beta$ -gal activity *in vivo* have been presented exploiting gadolinium contrast enhanced  $^1\text{H}$  magnetic resonance imaging (MRI) or  $^{19}\text{F}$  NMR,<sup>5–12</sup> optical,<sup>13–18</sup> and radionuclide imaging.<sup>19–21</sup> Traditional  $^{19}\text{F}$  NMR spectroscopy approaches have the advantage of detecting both the substrate and the product simultaneously,<sup>7–9</sup> but while imaging is feasible,<sup>22,23</sup> the achievable signal-to-noise has so far been insufficient for imaging in animals. By comparison,  $^1\text{H}$  MRI contrast can be far more sensitive, but the presence of substrate and the formation of product may not be readily identifiable due to tissue heterogeneity. We have demonstrated an Fe(III)-based  $^1\text{H}$  MRI approach using the commercially available black histological stain sodium 3,4-cyclohexenoesucletin- $\beta$ -D-galactopyranoside (S-Gal sodium salt) to detect  $\beta$ -gal activity in stably transfected *lacZ* expressing cancer cells *in vitro* and *in vivo* and this approach was also used to label and track stem cell localization.<sup>24,25</sup> It occurred to us that the approaches could be combined, whereby  $^{19}\text{F}$  NMR

spectroscopy would define substrate accumulation and conversion, while iron based  $^1\text{H}$  MRI contrast reveals regional enzyme activity.

*Escherichia coli* (*lacZ*)  $\beta$ -gal catalyzes the hydrolysis of  $\beta$ -D-galactopyranosides by cleavage of the C–O bond with  $\beta$ -configuration between D-galactose and the aglycone. Considering the multiple requirements for an enzyme responsive  $^{19}\text{F}/^1\text{H}$  MRI indicator, we chose salicylaldehyde nicotinoyl hydrazone, salicylaldehyde isonicotinoyl hydrazone, and salicylaldehyde benzoyl hydrazone as aroylhydrazone chelators based on reported characteristics.<sup>26–28</sup> A fluorine atom introduced at the *ortho* or *para* position to the  $\text{C}_{1(\text{gal})}$ -O bond in the salicylaldehyde fragment was expected to display a large  $^{19}\text{F}$  NMR chemical shift in response to cleavage by  $\beta$ -gal.<sup>29</sup>

We now report proof of principle using a fluorosalicylaldehyde aroylhydrazone  $\beta$ -D-galactopyranoside, which provides a  $^{19}\text{F}$  NMR signal sensitive to  $\beta$ -gal enzyme cleavage and the liberated aglycone spontaneously traps ferric ions generating  $^1\text{H}$  MRI contrast on  $T_2$ -weighted images (Figure 1). We currently add ferric ammonium citrate, but contrast could, in principle, develop from entrapment of endogenous  $\text{Fe}^{3+}$ .

### EXPERIMENTAL PROCEDURES

Detailed molecular characterization results based on chemical shift assignment and chemical analyses are provided in

Received: November 30, 2011

Revised: February 17, 2012

Published: February 18, 2012

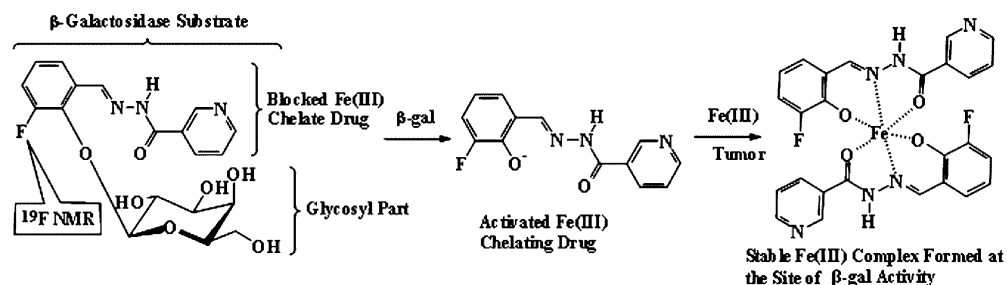


**Figure 1.** Proposed mode of action:  $\beta$ -galactosidase activity is detected by  $^{19}\text{F}$  NMR chemical shift accompanying release of aglycone and  $^1\text{H}$  MRI contrast induced by ferric ion complex.

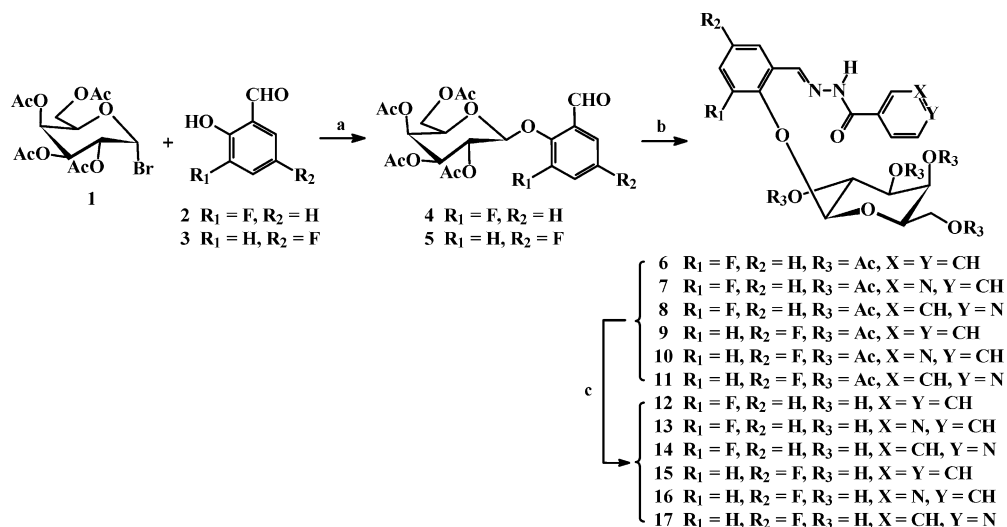


**Figure 2.** Reactions and the structures of 1–17. Reaction conditions: (a)  $\text{CH}_2\text{Cl}_2$ – $\text{H}_2\text{O}$ , pH 8–9, 50 °C, TBAB,  $\text{N}_2$ , 5–6 h, 92% ( $\rightarrow$ 4) or 86% ( $\rightarrow$ 5), respectively; (b) EtOH, AcOH (20  $\mu\text{L}$ ), benzoic hydrazide, nicotinic hydrazide or isoniazide (1.1 equiv), 80 °C,  $\text{N}_2$ , 4–5 h, 100% ( $\rightarrow$ 6), 90% ( $\rightarrow$ 7), 95% ( $\rightarrow$ 8), 95% ( $\rightarrow$ 9), 100% ( $\rightarrow$ 10), and 93% ( $\rightarrow$ 11) respectively; (c) 0.5 M  $\text{NH}_3$ –MeOH, 0 °C  $\rightarrow$  r.t., 24 h, quantitative yields.

Supporting Information. All *in vivo* studies were performed with approval from the Institutional Animal Care and Use Committee.

The synthetic route and structures of 1–17 are shown in Figure 2. Reaction of 2,3,4,6-tetra-*O*-acetyl- $\alpha$ -D-galactopyranosyl bromide 1 (Sigma Chemical Company, St Louis, MO) with 3- or 5-fluorosalicylaldehydes 2 or 3 at 50 °C catalyzed by tetrabutylammonium bromide (TBAB) in an aqueous dichloromethane biphasic system (pH 8–9) under  $\text{N}_2$  afforded 2-[(2',3',4',6'-tetra-*O*-acetyl- $\beta$ -D-galactopyranosyl)oxy]-3 or 5-fluorobenzaldehydes 4 or 5 in high yields (82–92%). Treatment of 4 or 5, respectively, with 1.1 equiv of benzoic hydrazide, nicotinic hydrazide, or isoniazid in acidic medium at 80 °C produced the corresponding 2-[(2',3',4',6'-tetra-*O*-acetyl- $\beta$ -D-galactopyranosyl)oxy]-3 or 5-fluorobenzaldehyde aroylhydrazones 6–11 in 90–100% yields, which were deacetylated with  $\text{NH}_3$ /MeOH from 0 °C to room temperature giving their free galactopyranosides 12–17 in quantitative yields.

**Detailed Syntheses.** 2-[(2',3',4',6'-Tetra-*O*-acetyl- $\beta$ -D-galactopyranosyl)oxy]-3 or 5-Fluoro-benzaldehydes 4–5.

**General Procedure.** A solution of 2,3,4,6-tetra-*O*-acetyl- $\alpha$ -D-galactopyranosyl bromide 1 (615 mg, 1.5 mmol) in  $\text{CH}_2\text{Cl}_2$  (10 mL) was added dropwise to a vigorously stirred biphasic mixture (pH 8–9) of 3- or 5-fluorosalicylaldehyde (2–3) (252 mg, 1.8 mmol) and tetrabutylammonium bromide (TBAB) (160 mg, 0.5 mmol) in  $\text{CH}_2\text{Cl}_2$ – $\text{H}_2\text{O}$  (20 mL, 1:1 v/v) over a period of 1 h at 50 °C under  $\text{N}_2$ , and the stirring continued for 4–5 h until TLC showed complete reaction. The products were extracted

with  $\text{CH}_2\text{Cl}_2$  (4  $\times$  25 mL), washed, dried ( $\text{Na}_2\text{SO}_4$ ), evaporated under reduced pressure to give a syrup, which was purified by column chromatography on silica gel to give 2-[(2',3',4',6'-tetra-*O*-acetyl- $\beta$ -D-galactopyranosyl)oxy]-3 or 5-fluorobenzaldehydes 4–5, as white crystals in >85% yield.

2-[(2',3',4',6'-Tetra-*O*-acetyl- $\beta$ -D-galactopyranosyl)oxy]-3 or 5-Fluorobenzaldehyde Aroylhydrazones 6–11. **General Procedure.** A solution of 2-[(2',3',4',6'-tetra-*O*-acetyl- $\beta$ -D-galactopyranosyl)oxy]-3 or 5-fluorobenzaldehyde 4 or 5 (200 mg, 0.44 mmol) in anhydrous EtOH (15 mL) containing AcOH (20  $\mu\text{L}$ ) was stirred vigorously respectively with benzoic hydrazide, nicotinic hydrazide, or isoniazid (0.48 mmol, 1.1 equiv) at 80 °C under  $\text{N}_2$  until TLC showed that the reaction was complete, then coevaporated with toluene to dryness *in vacuo*. Crystallization from EtOH– $\text{H}_2\text{O}$  or chromatography of the crude syrup on silica gel with appropriate eluents yielded the corresponding 2-[(2',3',4',6'-tetra-*O*-acetyl- $\beta$ -D-galactopyranosyl)oxy]-3 or 5-fluorobenzaldehyde aroylhydrazones 6–11 in 90–100% yields.

2-[( $\beta$ -D-Galactopyranosyl)oxy]-3 or 5-Fluorobenzaldehyde Aroylhydrazones 12–17. **General Procedure.** A solution of 2-[(2,3,4,6-tetra-*O*-acetyl- $\beta$ -D-galactopyranosyl)oxy]-3 or 5-fluorobenzaldehyde aroylhydrazones 6–11 (200 mg) in anhydrous MeOH (20 mL) containing 0.5 M  $\text{NH}_3$  was vigorously stirred from 0 °C to room temperature overnight until TLC showed complete reaction, then evaporated to dryness *in vacuo*. Chromatography of the crude syrup on silica gel with EtOAc–MeOH afforded

the corresponding free  $\beta$ -D-galactopyranosides 12–17 in quantitative yields.

**3-Fluorosallycylaldehyde Nicotinoyl Hydrazone (3-FBNH)-Hydrolysis Product of 13.** A solution of 3-fluorosallycylaldehyde (330 mg, 2.36 mmol) in anhydrous EtOH (15 mL) containing AcOH (20  $\mu$ L) was stirred vigorously with nicotinic hydrazide (323 mg, 2.36 mmol) at 80 °C under N<sub>2</sub> until TLC showed that the reaction was complete, then coevaporated with toluene to dryness *in vacuo*. Crystallization from EtOH-H<sub>2</sub>O yielded 3-FBNH (526 mg) as white needles.

**Fe:3-FBNH Complex.** To a solution of 3-FBNH (500 mg, 1.93 mmol) and Et<sub>3</sub>N (195 mg, 1.93 mmol) in anhydrous MeOH (100 mL) was added dropwise a solution of Fe(ClO<sub>4</sub>)<sub>3</sub>·6H<sub>2</sub>O (446 mg, 0.97 mmol) in anhydrous MeOH (50 mL) with stirring and gentle reflux under N<sub>2</sub> for 30 min. Upon cooling, a fine black precipitate was obtained, which was filtered, washed with EtOH then Et<sub>2</sub>O, and dried *in vacuo* yielding Fe-3-FBNH Complex [Fe(3-FBNH-H)<sub>2</sub>](ClO<sub>4</sub>)<sub>3</sub>·3H<sub>2</sub>O (576 mg) as black powder. Anal. Calcd. for C<sub>26</sub>H<sub>24</sub>ClFeN<sub>6</sub>O<sub>11</sub>F<sub>2</sub> (%): C, 43.03, H, 3.34, N, 11.59; Found: C, 42.95, H, 3.41, N, 11.48.

**Detection of  $\beta$ -Galactosidase by <sup>19</sup>F NMR in Solution.** 2-[( $\beta$ -D-galactopyranosyl)oxy]-3-fluorobenzaldehyde nicotinoyl hydrazone 13, 2-[( $\beta$ -D-galactopyranosyl)oxy]-3-fluorobenzaldehyde isonicotinoyl hydrazone 14 (2.11 mg, 5.0  $\mu$ mol), or 2-[( $\beta$ -D-galactopyranosyl)oxy]-5-fluorobenzaldehyde benzoylhydrazone 15 (2.10 mg, 5.0  $\mu$ mol) were dissolved in PBS (595  $\mu$ L) and a solution of  $\beta$ -gal (5  $\mu$ L, 1 unit/ $\mu$ L; E801A, Aldrich) was added. <sup>19</sup>F NMR time course spectra were acquired immediately at 376 MHz in 102 s each and continued at 37 °C over 4 h to assess relative rates of activity. 13 was also examined by <sup>19</sup>F MRI. In this case, 13 (7 mg) was dissolved in PBS/DMSO (250  $\mu$ L 1:1 mixture) at 37 °C and  $\beta$ -galactosidase (E801A 20 units) added. <sup>19</sup>F MR images were acquired at 376 MHz with 930  $\mu$ m in plane resolution across a 30 mm  $\times$  30 mm field of view and 10 mm slice thickness in 4 min 16 s each using 8 averages at each phase encode and TR = 1000 ms, TE = 1.6 ms, and 90° flip angle.

**<sup>1</sup>H MRI T<sub>2</sub> Maps of Phantoms of 13 and S-Gal in Agar.** Mixtures of agar and 3,4-cyclohexenoesculletin- $\beta$ -D-galactopyranoside sodium (S-Gal sodium salt, Sigma-Aldrich Inc., St. Louis, MO) (5 mM, 40  $\mu$ L) + ferric ammonium citrate (FAC 2.5 mM, 40  $\mu$ L) or 13 (5 mM, 40  $\mu$ L) + FAC (2.5 mM, 40  $\mu$ L) with or without  $\beta$ -gal (E801A, 5 units) were prepared in sections of 384 well plates cut to fit in a 1 turn, 2 cm volume solenoid coil. T<sub>2</sub> maps were acquired at 4.7 T using a spin echo sequence with variable echo times. MRI parameters were: FOV = 40 mm  $\times$  40 mm, matrix 128  $\times$  128, slice thickness = 1 mm, TR = 6 s, TE = 10, 20, 30, 50, 80, 100, 150, and 200 ms.

**Detection of  $\beta$ -Galactosidase by <sup>19</sup>F NMR in Cells.** Human MCF7 breast and PC3 prostate cancer cells were transfected to stably express the *E. coli lacZ* gene constitutively, as described previously.<sup>8,9</sup> Wild-type and -*lacZ* cells were grown in culture dishes under standard conditions and harvested for NMR tests. <sup>19</sup>F NMR spectra were acquired at 9.4 T up to 40 h after addition of 13 (2.11 mg, 5.0  $\mu$ mol) to MCF7 cells (5.0  $\times$  10<sup>6</sup>) in 600  $\mu$ L PBS, and in some cases, Fe<sup>3+</sup> (FAC 2.5  $\mu$ mol) was added. In addition to evaluating intact cells, additional tests were conducted with lysed cells. For comparison, equal numbers of cells were prepared for evaluation intact or following lysis. Cell lysis was achieved by a freeze/thaw method: equal numbers of MCF7-*lacZ* or PC3-*lacZ* cells were suspended in PBS and then frozen at -80 °C for 10 min before thawing at room temperature over 3 cycles.

**In Vivo MR Studies.** PC3 cells (wild type or transfected to stably express *lacZ*<sup>8</sup>) were implanted subcutaneously in thighs of SCID mice (*n* = 3). NMR studies were performed at 4.7 T using a Varian Unity INOVA horizontal bore scanner (200.1 MHz for <sup>1</sup>H, 188.2 MHz <sup>19</sup>F). When the tumors reached ~0.8 cm in diameter, mice were anesthetized (isoflurane/air) and placed on a platform with the tumor-bearing leg inserted into a 2-cm-diameter home-built volume coil (tunable from 200.1 MHz for <sup>1</sup>H to 188.2 MHz for <sup>19</sup>F). The animal temperature was maintained at 37 °C by a warm pad with circulating water. The mouse bed was inserted into the bore of the MR scanner and shimming was performed on the tissue water proton signal. T<sub>1</sub> and T<sub>2</sub> maps of the tumor were measured using a spin echo sequence with varying repetition and echo times (acquisition parameters: field of view (FOV) 50 mm  $\times$  50 mm, matrix 128  $\times$  128, slice thickness 1 mm, 15 slices). The mouse-bearing platform was removed from the magnet and a solution of 13 (50  $\mu$ L 50 mM, DMSO/PBS 1:1 v/v) was injected directly into the tumor in a “fan” pattern. The platform was replaced in the magnet and <sup>19</sup>F NMR spectra were obtained immediately after retuning the coil to the <sup>19</sup>F resonance frequency. Each spectrum was acquired in 166 s (acquisition parameters: pulse width 45  $\mu$ s, 128 acquisitions, spectral width 100 ppm, 60 Hz exponential line broadening). The mouse-bearing platform was again removed from the magnet and a solution of FAC (50  $\mu$ L 50 mM, PBS) was now injected directly into the tumor in a similar pattern to 13. <sup>19</sup>F NMR spectra were obtained and the coil was retuned to the <sup>1</sup>H frequency, and new T<sub>1</sub> and T<sub>2</sub> maps were acquired. For analysis, regions with injected contrast agent were identified based on the T<sub>2</sub>- and T<sub>1</sub>-weighted images (to delineate tumor boundary and locate the injected Fe<sup>3+</sup> ions, respectively). For one animal, no injection site could be identified inside the tumor and hence the data for this tumor were not used. To confirm  $\beta$ -gal activity in tumors, tissues were embedded in Tissue-Tek OCT (Miles Laboratory, Elkhart, IN, USA), and frozen in liquid nitrogen. Cryostat sections (8  $\mu$ m) were collected on gelatin-coated glass slides and stained with X-gal and eosin (Sigma) for  $\beta$ -gal activity.

**Testing Product Aglycone Visibility in Vivo.** A mixture of sodium trifluoroacetate (50 mM) and aglycone (3-FBNH (3 or 6 mg in total volume 50  $\mu$ L or 100  $\mu$ L of a 3:1 mixture of DMSO:PBS) was injected into muscle of three adult 129S-Gt(ROSA)26Sor/J mice (2 live and 2 post mortem). <sup>19</sup>F NMR spectra were acquired immediately at 4.7 T and every 2 min. NaTFA served as a chemical shift reference at 0 ppm.

## RESULTS

Each of the target reporter molecules was achieved in high yield and structures were confirmed by NMR and chemical analyses (see Supporting Information). The anomeric  $\beta$ -D-configuration of compounds 4–17 in the <sup>4</sup>C<sub>1</sub> chair conformation was confirmed by the observed <sup>1</sup>H NMR chemical shifts ( $\delta$ <sub>H</sub> 4.79–5.12 ppm) of the anomeric protons and the J<sub>1,2</sub> (*J* ~8 Hz) and J<sub>2,3</sub> (*J* ~10 Hz) coupling constants.<sup>29</sup> The anomeric carbon resonances appeared at  $\delta$ <sub>C-1'</sub> 100.05–105.23 ppm in accord with the  $\beta$ -D-configuration. <sup>19</sup>F NMR chemical shifts were measured with respect to sodium trifluoroacetate (NaTFA,  $\delta$  = 0 ppm) in a capillary as an external standard. 12–17 each gave a single narrow <sup>19</sup>F NMR signal between  $\delta$ <sub>F</sub> -44.0 and -55.0 ppm (Table 1) essentially invariant ( $\Delta\delta$ <sub>F</sub>  $\leq$  0.05 ppm) with pH in the range 3–12 and temperatures from 25 to 37 °C in 0.9% saline or rabbit whole blood.

**Table 1.**  $^{19}\text{F}$  NMR Chemical Shifts (ppm) of 12–17 and Hydrolytic Rates ( $\mu\text{mol}/\text{min}/\text{unit}$ ) of 13–15 with  $\beta\text{-gal}^a$ 

No.	12	13	14	15	16	17
$\delta_{\text{F}}$ (substrate)	-54.84	-54.62	-54.60	-44.38	-45.02	-45.03
$\delta_{\text{F}}$ (aglycone)	---	-62.27	-62.03	-49.61	---	---
$\Delta\delta_{\text{F}}$	---	7.65	7.43	5.23	---	---
$\nu$ ( $\mu\text{mol}/\text{min}/\text{unit}$ )	---	3.91	1.67	0.55	---	---

$^a\beta\text{-gal}$  (E801A) at 37 °C in PBS (0.1 M, pH = 7.4).

When  $\beta\text{-gal}$  (E801A) was added to 12–17 in phosphate buffered saline (PBS) at 37 °C, only 13–15 were hydrolyzed releasing the 3- or 5-fluorobenzaldehyde aroylhydrazones appearing also as single narrow  $^{19}\text{F}$  signals shifted upfield between  $\Delta\delta_{\text{F}} = 5.23\text{--}7.65$  ppm ( $\delta_{\text{F}}$  -49.0 to -63.0 ppm) (Figures 3 and

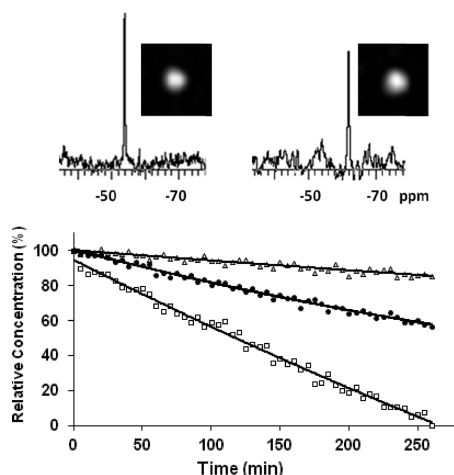
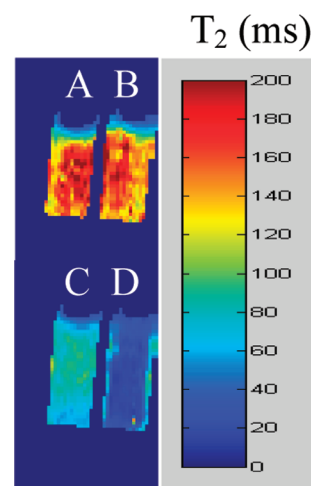


Figure 3). Substrate response to  $\beta\text{-galactosidase}$ . Graph shows the loss of each of the three agents 13–15 ( $5.0 \mu\text{mol}$ ;  $\square$ , 13;  $\bullet$ , 14;  $\Delta$ , 15) when incubated with  $\beta\text{-galactosidase}$  (E801A, 5 units) in PBS (0.1 M, 600  $\mu\text{L}$ ) at 37 °C, as detected by  $^{19}\text{F}$  NMR spectroscopy revealing that 13 reacts fastest. When  $\beta\text{-galactosidase}$  (20 units) was added to a solution of 13 (7 mg 16.5  $\mu\text{mol}$ ) in 250  $\mu\text{L}$  PBS/DMSO 1:1 at 37 °C, conversion was detectable by  $^{19}\text{F}$  NMR spectroscopy and imaging at 9.4 T (376 MHz: baseline at left and after 2.5 h at right) showing product 3-fluorobenzaldehyde nicotinoyl hydrazone (3-FBNH).

S1; Table 1), which is comparable to shifts reported previously for  $^{19}\text{F}$  NMR gene reporter molecules.<sup>7–9,29,30</sup> The hydrolysis of 13–15 proceeded smoothly indicating that the liberated aglycones 3- or 5-fluorobenzaldehyde aroylhydrazones had no inhibitory effects on  $\beta\text{-gal}$ , and the shapes of the kinetic curves suggest straightforward zero-order kinetics. The rate of reaction of 13 ( $\nu_{(\text{E801A})} = 3.91 \mu\text{mol}/\text{min}/\text{unit}$ ) was comparable to that reported previously for 3-*O*-( $\beta$ -D-galactopyranosyl)-6-fluoropyridoxol (GFPOL)<sup>30</sup> and much faster than the other molecules here, so it was chosen for further studies. Enzyme induced hydrolysis was also observable by  $^{19}\text{F}$  MRI (Figure 3). Titration of product 3-fluorobenzaldehyde nicotinoyl hydrazone (3-FBNH) showed a small chemical shift ( $\sim 0.5$  ppm) in the pH range 6.5–7.7 (Figure S2).

Proton MRI of agar phantoms of 13 or commercial S-Gal (3,4-cyclohexenoesucletin  $\beta$ -D-galactopyranoside) with ferric ions showed very similar  $T_2$  ( $152 \pm 21$  ms vs  $156 \pm 25$  ms; Figure 4). Incorporation of  $\beta\text{-gal}$  in the agar yielded much reduced  $T_2$  values and the difference was much greater for 13 than S-Gal ( $23 \pm 12$  ms vs  $78 \pm 11$  ms: alternately,  $\Delta R_2$   $36.9 \text{ s}^{-1}$  vs  $6.4 \text{ s}^{-1}$ ). By analogy with S-Gal,<sup>24</sup> we attribute the relaxation



**Figure 4.**  $^1\text{H}$  MRI  $T_2$  maps of phantoms of 13 and S-Gal in agar. Comparison of  $T_2$  shortening due to addition of  $\beta\text{-gal}$  enzyme to commercial substrate S-Gal or 13. (A) S-Gal (5 mM) +  $\text{Fe}^{3+}$  (2.5 mM); (B) 13 (5 mM) +  $\text{Fe}^{3+}$  (2.5 mM); (C) as (A) +  $\beta\text{-gal}$  (E801A, 5 units); (D) as (B) +  $\beta\text{-gal}$  (E801A, 5 units).

enhancement to formation of complex between 3-FBNH and  $\text{Fe}^{3+}$ . Chemical analysis indicated a 1:2  $\text{Fe}^{3+}$ :3-FBNH complex.

When 13 was incubated with MCF7 human breast tumor cells for 5 h in PBS at 37 °C under 5%  $\text{CO}_2$  in air, no changes were observed in the  $^{19}\text{F}$  NMR spectrum. Addition of 13 to stably transfected MCF7-*lacZ* cells led to cleavage in a smooth monotonic manner with a rate of  $0.25 \mu\text{mol}/\text{min}$  per million cells, and appearance of a new  $^{19}\text{F}$  signal of the released aglycone 3-fluorobenzaldehyde nicotinoyl hydrazone (3-FBNH) around  $-62.27$  ppm (Figure 5). When ferric ammonium citrate (FAC) was added after 28 h, the product aglycone  $^{19}\text{F}$  signal immediately disappeared, which we attribute to a paramagnetic relaxation enhancement in the  $\text{Fe}^{3+}$ :3-FBNH complex.

Given that conversion of substrate appeared much slower in cells than with enzyme *in vitro*, tests were conducted to compare intact and lysed cells. Incubation of 13 with equal numbers of intact or lysed MCF7-*lacZ* cells showed 25% conversion after overnight incubation (14 h), whereas lysed cells showed 75%. Similarly, PC3-*lacZ* cells showed only 15% conversion, while lysed PC3-*lacZ* cells showed 85%.

As an initial proof of principle, 13 and FAC were injected into wild type (WT) and *lacZ*-transfected PC3 human prostate tumor xenografts growing in mice (Figure 6). Spin-lattice relaxation time ( $T_1$ )-weighted images showed a local hyperintensity associated with the ferric ions, and a corresponding drop in the  $T_1$  values was observed. For groups of tumors, there was no significant difference between mean baseline  $T_1$  ( $2.4 \pm 0.4$  s;  $n = 2$  WT vs  $2.4 \pm 0.3$  s;  $n = 3$  *lacZ*;  $p > 0.8$ ). Following injection of contrast agent (i.e., 13 plus FAC),  $T_1$  decreased in WT tumors ( $T_1 = 1.5 \pm 0.4$ ,  $p < 0.2$ ), but the change was significant in *lacZ* tumors ( $T_1 = 1.1 \pm 0.4$ ;  $p < 0.01$ ). For the

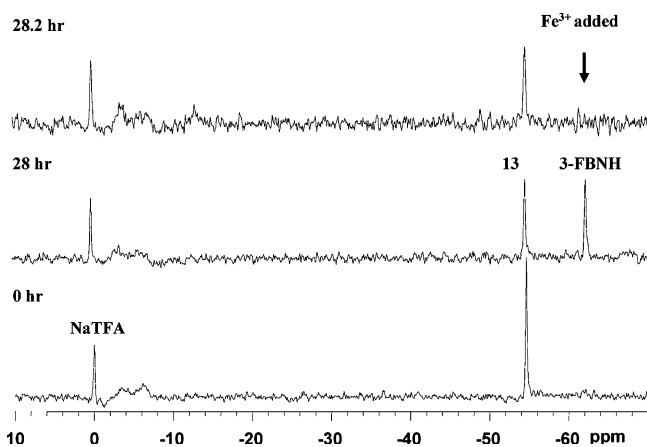


**Figure 5.** Detection of  $\beta$ -gal activity in cultured cells. 376 MHz  $^{19}\text{F}$  NMR spectra of **13** (2.11 mg,  $5.0\ \mu\text{mol}$ ) after addition to stably transfected MCF7-*lacZ* cells ( $5.0 \times 10^6$ ).  $\text{Fe}^{3+}$  ( $2.5\ \mu\text{mol}$ ) was added after 28 h. Each spectrum was acquired in 205 s, and enhanced with an exponential line broadening 40 Hz.

same regions of the tumors, a large signal decrease was observed in spin–spin ( $T_2$ )-weighted  $^1\text{H}$  images in PC3-*lacZ* tumors only at the injection site.  $T_2$  was similar before injection of contrast agent ( $T_2 = 55 \pm 5\ \text{ms}$  (*lacZ*) vs  $T_2 = 52 \pm 16\ \text{ms}$  (WT)). Following administration of contrast agent,  $T_2$  changed significantly in *lacZ* tumors ( $T_2 = 39 \pm 5\ \text{ms}$ ;  $p < 0.05$ ), but not in WT tumors ( $T_2 = 53 \pm 15\ \text{ms}$ ;  $p > 0.9$ ).  $^{19}\text{F}$  spectroscopy showed the presence of substrate **13** in the WT tumors, which decreased slowly (Figure 7), but no aglycone product. In corresponding PC3-*lacZ* tumors, no substrate or product signal was observed by  $^{19}\text{F}$  NMR. Enzyme activity was confirmed postmortem based on X-gal staining of slices of PC3-*lacZ* tumors, which turned intense blue, whereas wild-type tumors showed no blue color (Figure 6).

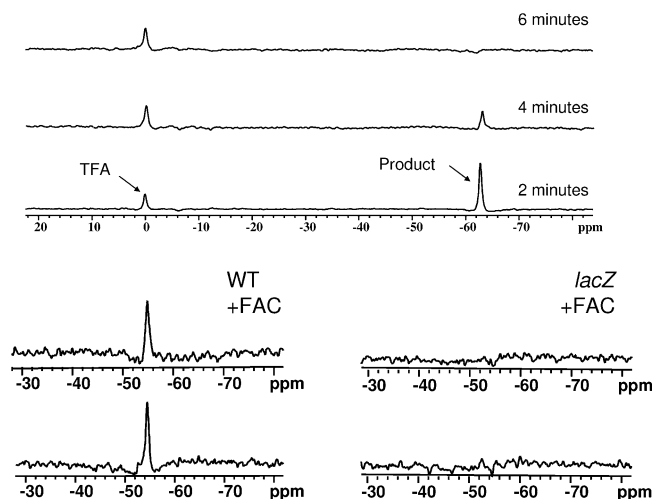


**Figure 7.** Detection of  $\beta$ -gal activity *in vivo* by  $^{19}\text{F}$  NMR. Left: Following injection of **13** (1 mg) into a PC3-WT tumor,  $^{19}\text{F}$  NMR spectroscopy showed substrate at  $-54.6\ \text{ppm}$  with respect to sodium trifluoroacetate reference (lower spectrum). Following injection of 0.6 mg FAC, the substrate remained visible (upper left). Spectra were acquired in about 2½ min and enhanced with 60 Hz exponential line broadening prior to Fourier transformation giving a SNR of 35. Right: Similar injection into PC3-*lacZ* tumor showed minimal  $^{19}\text{F}$  NMR signal and there was minimal change after addition of FAC (upper). Upper spectra: A mixture of sodium trifluoroacetate and aglycone (**3-FBNH**; 3 mg) in total volume of  $50\ \mu\text{L}$  was injected into muscle of a dead adult 129S-Gt(ROSA)26Sor/J mouse.  $^{19}\text{F}$  NMR spectra were acquired immediately and every 2 min. NaTFA served as a chemical shift reference at 0 ppm and remained quite constant. Meanwhile aglycone was initially seen with SNR = 194 at  $-62.8\ \text{ppm}$ , but signal decreased and was no longer observed after 6 min.

Lack of detectable  $^{19}\text{F}$  NMR could have been caused by clearance of the product from *lacZ* tumors *in vivo* or potentially precipitation of the product by association with ferric ions,

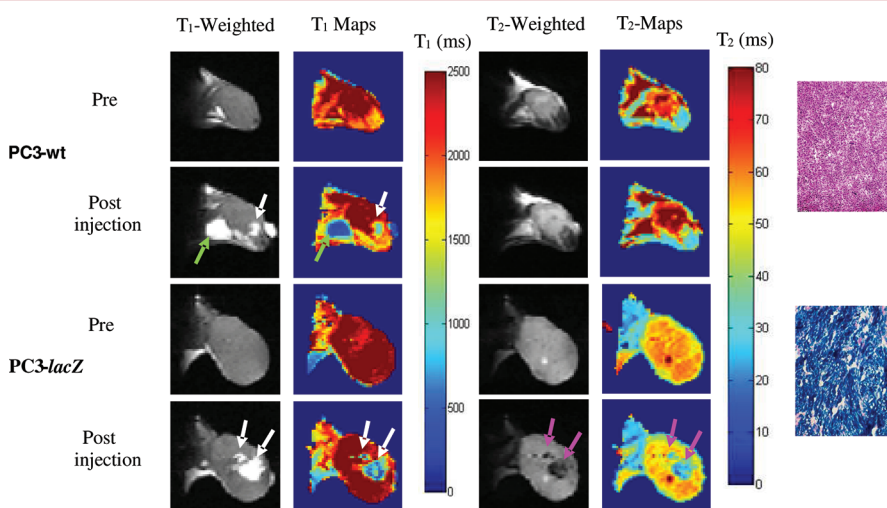


**Figure 6.** Imaging  $\beta$ -gal activity *in vivo*. *In vivo* study showing *lacZ* gene-reporter activity detected by  $^1\text{H}$  MRI in representative PC3 tumor xenografts in SCID mice after intratumoral injection ( $100\ \mu\text{L}$  total volume) of ferric ammonium citrate (FAC) and **13**. The presence of FAC + **13** is seen in  $T_1$ -weighted images (TR/TE = 300/12 ms) and  $T_1$  maps (white arrows) in both wild-type tumors (columns 1 and 2, row 2) and *lacZ* tumors (columns 1 and 2, row 4). Baseline tumor  $T_1 = 2.8 \pm 0.1\ \text{s}$  for *lacZ* and  $2.6 \pm 0.2\ \text{s}$  for WT, versus  $1.1 \pm 0.6\ \text{s}$  for *lacZ* and  $1.8 \pm 0.5\ \text{s}$  for WT following injection of **13** + FAC. Significant change in  $T_2$ -weighted images (TR/TE = 6000/50 ms, column 3, row 4) and  $T_2$  values (column 4, row 4) was seen only in the *lacZ*-transfected tumors post-injection of FAC and **13** (pink arrows). Baseline  $T_2 = 56 \pm 4\ \text{ms}$  for *lacZ* and  $T_2 = 63 \pm 7\ \text{ms}$  for WT became  $T_2 = 34 \pm 10\ \text{ms}$  for *lacZ* and  $T_2 = 63 \pm 18\ \text{ms}$  for WT. Green arrow indicates anomalous injection outside tumor, and this region was excluded from analysis. Histological sections at right (original magnification  $\times 100$ ) confirm intense  $\beta$ -gal expression in *lacZ* tumor based on X-gal and H&E staining (blue, lower slide) with essentially no activity in WT tumor (pink, upper slide).

rendering it NMR invisible. To gain further insight into the lack of  $^{19}\text{F}$  signal, product aglycone was injected into muscle of ROSA26 mice, which express *lacZ* throughout their bodies. Internal NaTFA standard and aglycone were immediately detectable, but over a few minutes, the aglycone signal at  $-61.5$  ppm disappeared in both live and dead mice, while TFA remained visible in the dead animal (Figure 7).

## DISCUSSION

We have demonstrated a novel dual  $^{19}\text{F}/^1\text{H}$  MR *lacZ* gene detection approach by introducing a fluorine atom into iron-chelating aroylhydrazone aglycones of  $\beta$ -D-galactopyranosides. When activated by  $\beta$ -gal, the released fluoroaroylhydrazones display a distinct chemical shift with respect to the substrate and can be spontaneously trapped by  $\text{Fe}^{3+}$  at the site of enzyme activity forming highly relaxing complexes *in situ*. The complexes cause strong  $T_2$  relaxation, providing  $^1\text{H}$  MRI contrast to reveal *lacZ* expression.

We believe the  $T_1$  contrast following injection is attributable to free ferric ions from FAC and this was observed in both WT and *lacZ* tumors (Figure 6). However,  $\beta$ -gal activity was clearly revealed by the colocalized hypointensity in  $T_2$ -weighted images and corresponding significant shortening in  $T_2$ , whereas no  $T_2$  contrast was observed for WT tumors.

The utility of a reporter molecule is predicated on a reasonable rate of activity. The conversion rates *in vitro* were very slow (Figure 3). Aglycone was released much more rapidly by lysed MCF7-*lacZ* or PC3-*lacZ* cells indicating that cell permeation is a strong barrier to activity. However, contrast was observed almost immediately in *lacZ* tumors upon direct intratumoral injection. Such differential rates of activity have also been reported for  $^{19}\text{F}$  reporters.<sup>8,9</sup> The ultimate goal is development of reporter molecules which may be administered systemically. At this stage, the method requires direct intratumoral injection, but we note that this limitation has also been encountered by most other reports regarding reporter molecules for  $\beta$ -gal using NMR, radionuclides, or photoacoustic tomography.<sup>8,9,12,16,21,24</sup> To date, systemic administration has generally been restricted to optical imaging approaches<sup>14,18,31</sup> and a single report regarding a Gd-based contrast agent.<sup>6</sup>

Ideally,  $^{19}\text{F}$  NMR would show both substrate and product, and this was observed in cells (Figure 5). However, the liberated product signal was absent in the presence of ferric ions and *in vivo*. This could be attributed to clearance of the product from *lacZ* tumors and ROSA26 muscle *in vivo*, but the post-mortem test in the ROSA26 mouse also indicated signal disappearance over a period of 6 min consistent with precipitation of the product (possibly in association with endogenous ferric ions), which renders it NMR invisible.  $^{19}\text{F}$  signal for TFA remained visible over this time. The  $^{19}\text{F}$  NMR is able to locate substrate, but not product, and we are seeking alternate molecules, which can reveal both substrate and product.

In the present studies, we added exogenous ferric ions, but we note that cancer cells often exhibit elevated iron levels and a number of Fe-chelators have been proposed for cancer therapy.<sup>32</sup> Indeed, aroyl hydrazones are in clinical use as ferric ion scavenging agents<sup>33</sup> suggesting a potential for clinical theranostic application. There is an extensive literature on aroyl hydrazones regarding thermodynamic characteristics of ferric ion complexes,<sup>26,28</sup> and we assume that  $^{19}\text{F}$  analogues presented here behave similarly. We were not able to obtain a crystal structure of the complex, but chemical analysis confirmed a 2:1 structure.

$^{19}\text{F}$  NMR is gaining popularity as a reporter for diverse enzyme reactions based on various strategies. The simplest is change in chemical shift that we and others have exploited extensively.<sup>8,9,34,35</sup> More recently, differential relaxation rates have been exploited based on paramagnetic relaxation enhancement (PRE)<sup>10,36</sup> or differential restricted mobility<sup>37,38</sup> to reveal enzyme activity based on changes in line broadening. In addition, several recent reports have presented bimodal reporter strategies revealing enzyme activity based on  $^{19}\text{F}$  NMR and fluorescence.<sup>38,39</sup>

Ultimately, we hope to develop this approach for systemic delivery of reporter molecules, but direct injection into the tissues of interest already demonstrates selective detection of *lacZ* expression versus WT. The multimodality approach represents a new paradigm exploiting  $^{19}\text{F}$  NMR together with both  $T_1$  and  $T_2$   $^1\text{H}$  MRI contrast to reveal the presence or absence of enzyme activity. The observations are in accord with renewed excitement and innovations in  $^{19}\text{F}$  NMR notably for detecting enzyme activity.<sup>37,39-42</sup>

## ASSOCIATED CONTENT

### Supporting Information

Experimental details and molecular characterization. This material is available free of charge via the Internet at <http://pubs.acs.org>.

## AUTHOR INFORMATION

### Corresponding Author

\*Phone: (214)-648-8926. Fax: (214)-648-4538. E-mail: Ralph.Mason@UTSouthwestern.edu.

### Present Address

†Currently at the School of Biological and Health Systems Engineering, Arizona State University, Tempe, AZ

### Notes

The authors declare no competing financial interest.

## ACKNOWLEDGMENTS

Supported in part by NCI R21 CA120774, DOD Breast Cancer Initiative IDEA award DAMD17-03-1-0343, and the Small Animal Imaging Research Program, which is supported in part by NCI U24 CA126608 and P30 CA142543. NMR experiments were conducted at the Advanced Imaging Research Center, an NIH BTRP facility (P41-RR02584). We are grateful to Praveen K. Gulaka, Jennifer Magnusson, Jennifer McAnally, and Ya Ren for expert technical assistance.

## REFERENCES

- (1) Gilad, A. A.; Winnard, P. T.; van Zijl, P. C. M.; and Bulte, J. W. M. (2007) Developing MR reporter genes: promises and pitfalls. *NMR Biomed.* 20, 275–290.
- (2) Razgulina, A., Ma, N., and Rao, J. H. (2011) Strategies for *in vivo* imaging of enzyme activity: an overview and recent advances. *Chem. Soc. Rev.* 40, 4186–4216.
- (3) Kruger, A., Schirmacher, V., and Khokha, R. (1998) The bacterial *lacZ* gene: An important tool for metastasis research and evaluation of new cancer therapies. *Cancer Metast. Rev.* 17, 285–94.
- (4) de Almeida, R. A., Burgess, D., Shema, R., Motlekar, N., Napper, A. D., Diamond, S. L., and Pavitt, G. D. (2008) A *Saccharomyces cerevisiae* cell-based quantitative beta-galactosidase handling and assay compatible with robotic high-throughput screening. *Yeast* 25, 71–76.
- (5) Louie, A. Y., Huber, M. M., Ahrens, E. T., Rothbacher, U., Moats, R., Jacobs, R. E., Fraser, S. E., and Meade, T. J. (2000) *In vivo*

visualization of gene expression using magnetic resonance imaging. *Nat. Biotechnol.* 18, 321–325.

(6) Chang, Y. T., Cheng, C. M., Su, Y. Z., Lee, W. T., Hsu, J. S., Liu, G. C., Cheng, T. L., and Wang, Y. M. (2007) Synthesis and characterization of a new bioactivated paramagnetic gadolinium(III) complex [Gd(DOTA-FPG)(H<sub>2</sub>O)] for tracing gene expression. *Bioconjugate Chem.* 18, 1716–1727.

(7) Cui, W., Otten, P., Li, Y., Koeneman, K., Yu, J., and Mason, R. P. (2004) A novel NMR approach to assessing gene transfection: 4-fluoro-2-nitrophenyl- $\beta$ -D-galactopyranoside as a prototype reporter molecule for  $\beta$ -galactosidase. *Magn. Reson. Med.* 51, 616–20.

(8) Liu, L., Kodibagkar, V. D., Yu, J.-X., and Mason, R. P. (2007) <sup>19</sup>F-NMR detection of lacZ gene expression via the enzymic hydrolysis of 2-fluoro-4-nitrophenyl  $\beta$ -D-galactopyranoside *in vivo* in PC3 prostate tumor xenografts in the mouse. *FASEB J.* 21, 2014–2019.

(9) Yu, J. X., Kodibagkar, V. D., Liu, L., and Mason, R. P. (2008) A <sup>19</sup>F NMR Approach using Reporter Molecule Pairs to Assess  $\beta$ -Galactosidase in Human Xenograft Tumors *In Vivo*. *NMR Biomed.* 21, 704–12.

(10) Mizukami, S., Matsushita, H., Takikawa, R., Sugihara, F., Shirakawa, M., and Kikuchi, K. (2011) <sup>19</sup>F MRI detection of  $\beta$ -galactosidase activity for imaging of gene expression. *Chem. Sci.* 2, 1151–1155.

(11) Hanaoka, K., Kikuchi, K., Terai, T., Komatsu, T., and Nagano, T. (2008) A Gd<sup>3+</sup>-based magnetic resonance imaging contrast agent sensitive to beta-galactosidase activity utilizing a receptor-induced magnetization enhancement (RIME) phenomenon. *Chem.—Eur. J.* 14, 987–995.

(12) Arena, F., Singh, J. B., Gianolio, E., Stefania, R., and Aime, S. (2011) beta-Gal Gene Expression MRI Reporter in Melanoma Tumor Cells. Design, Synthesis, and *In Vitro* and *In Vivo* Testing of a Gd(III) Containing Probe Forming a High Relaxivity, Melanin-Like Structure upon beta-Gal Enzymatic Activation. *Bioconjugate Chem.* 22, 2625–2635.

(13) Kamiya, M., Kobayashi, H., Hama, Y., Koyama, Y., Bernardo, M., Nagano, T., Choyke, P. L., and Urano, Y. (2007) An enzymatically activated fluorescence probe for targeted tumor imaging. *J. Am. Chem. Soc.* 129, 3918–3929.

(14) Tung, C. H., Zeng, Q., Shah, K., Kim, D. E., Schellingerhout, D., and Weissleder, R. (2004) *In vivo* imaging of beta-galactosidase activity using far red fluorescent switch. *Cancer Res.* 64, 1579–83.

(15) Jossierand, V., Texier-Nogues, I., Huber, P., Favrot, M. C., and Coll, J. L. (2007) Non-invasive *in vivo* optical imaging of the lacZ and luc gene expression in mice. *Gene Ther.* 14, 1587–1593.

(16) Li, L., Zemp, R. J., Lungu, G., Stoica, G., and Wang, L. H. V. (2007) Photoacoustic imaging of lacZ gene expression *in vivo*. *J. Biomed. Optics* 12, 020504.

(17) Kamiya, M., Asanuma, D., Kuranaga, E., Takeishi, A., Sakabe, M., Miura, M., Nagano, T., and Urano, Y. (2011) beta-Galactosidase Fluorescence Probe with Improved Cellular Accumulation Based on a Spirocyclized Rhodol Scaffold. *J. Am. Chem. Soc.* 133, 12960–12963.

(18) Liu, L., and Mason, R. P. (2010) Imaging beta-Galactosidase Activity in Human Tumor Xenografts and Transgenic Mice Using a Chemiluminescent Substrate. *PLoS One* 5, e12024.

(19) Lee, K. H., Byun, S. S., Choi, J. H., Paik, J. Y., Choe, Y. S., and Kim, B. T. (2004) Targeting of lacZ reporter gene expression with radioiodine-labelled phenylethyl-beta-D-thiogalactopyranoside. *Eur. J. Nucl. Med. Mol. Imaging* 31, 433–8.

(20) Celen, S., Deroose, C., de Groot, T., Chitneni, S. K., Gijssbers, R., Debyser, Z., Mortelmans, L., Verbruggen, A., and Bormans, G. (2008) Synthesis and evaluation of F-18- and C-11-labeled phenyl-galactopyranosides as potential probes for *in vivo* visualization of LacZ gene expression using positron emission tomography. *Bioconjugate Chem.* 19, 441–449.

(21) Van Dort, M. E., Lee, K. C., Hamilton, C. A., Rehemtulla, A., and Ross, B. D. (2008) Radiosynthesis and Evaluation of 5-[I-125]-Iodindol-3-yl-beta-D-Galactopyranoside as a beta-Galactosidase Imaging Radioligand. *Mol. Imaging* 7, 187–197.

(22) Kodibagkar, V. D., Yu, J., Liu, L., Hetherington, H. P., and Mason, R. P. (2006) Imaging  $\beta$ -galactosidase activity using <sup>19</sup>F chemical shift imaging of LacZ gene-reporter molecule 2-fluoro-4-nitrophenol- $\beta$ -D-galactopyranoside. *Magn. Reson. Imaging* 24, 959–962.

(23) Yu, J. X., Liu, L., Kodibagkar, V. D., Cui, W., and Mason, R. P. (2006) Synthesis and Evaluation of Novel Enhanced Gene Reporter Molecules: Detection of b-Galactosidase Activity Using <sup>19</sup>F NMR of Trifluoromethylated Aryl  $\beta$ -D-Galactopyranosides. *Bioorg. Med. Chem.* 14, 326–33.

(24) Cui, W., Liu, L., Kodibagkar, V. D., and Mason, R. P. (2010) S-Gal®, A novel <sup>1</sup>H MRI reporter for  $\beta$ -galactosidase. *Magn. Reson. Med.* 64, 65–71.

(25) Bengtsson, N. E., Brown, G., Scott, E. W., and Walter, G. A. (2010) lacZ as a Genetic Reporter for Real-Time MRI. *Magn. Reson. Med.* 63, 745–753.

(26) Dubois, J. E., Fakhryan, H., Doucet, J. P., and Chahine, J. M. E. (1992) Kinetic and Thermodynamic Study of Complex-Formation between Iron(II) and Pyridoxal Isonicotinoylhydrazone and Other Synthetic Chelating-Agents. *Inorg. Chem.* 31, 853–859.

(27) Kalinowski, D. S., and Richardson, D. R. (2005) The Evolution of Iron Chelators for the Treatment of Iron Overload Disease and Cancer. *Pharmacol. Rev.* 57, 547–583.

(28) Yu, Y., Kalinowski, D. S., Kovacevic, Z., Siafakas, A. R., Jansson, P. J., Stefani, C., Lovejoy, D. B., Sharpe, P. C., Bernhardt, P. V., and Richardson, D. R. (2009) Thiosemicarbazones from the Old to New: Iron Chelators That Are More Than Just Ribonucleotide Reductase Inhibitors. *J. Med. Chem.* 52, 5271–5294.

(29) Yu, J. X., Otten, P., Ma, Z., Cui, W., Liu, L., and Mason, R. P. (2004) A Novel NMR Platform for Detecting Gene Transfection: Synthesis and Evaluation of Fluorinated Phenyl  $\beta$ -D-Galactosides with Potential Application for Assessing LacZ Gene Expression. *Bioconjugate Chem.* 15, 1334–1341.

(30) Yu, J. X., Ma, Z., Li, Y., Koeneman, K. S., Liu, L., and Mason, R. P. (2005) Synthesis and Evaluation of a Novel Gene Reporter Molecule: Detection of  $\beta$ -galactosidase activity Using <sup>19</sup>F NMR of a Fluorinated Vitamin B6 conjugate. *Med. Chem.* 1, 255–262.

(31) Wehrman, T. S., von Degenfeld, G., Krutzik, P., Nolan, G. P., and Blau, H. M. (2006) Luminescent imaging of beta-galactosidase activity in living subjects using sequential reporter-enzyme luminescence. *Nat. Methods* 3, 295–301.

(32) Whitnall, M., Howard, J., Ponka, P., and Richardson, D. R. (2006) A class of iron chelators with a wide spectrum of potent antitumor activity that overcomes resistance to chemotherapeutics. *Proc. Natl. Acad. Sci. U.S.A.* 103, 14901–14906.

(33) Richardson, D. R., Kalinowski, D. S., Lau, S., Jansson, P. J., and Lovejoy, D. B. (2009) Cancer cell iron metabolism and the development of potent iron chelators as anti-tumour agents. *Biochim. Biophys. Acta* 1790, 702–717.

(34) Yu, J. X., Kodibagkar, V., Cui, W., and Mason, R. P. (2005) <sup>19</sup>F: a versatile reporter for non-invasive physiology and pharmacology using magnetic resonance. *Curr. Med. Chem.* 12, 818–848.

(35) Dresselaers, T., Theys, J., Nuyts, S., Wouters, B., de Bruijn, E., Anne, J., Lambin, P., Van Hecke, P., and Landuyt, W. (2003) Non-invasive F-19 MR spectroscopy of 5-fluorocytosine to 5-fluorouracil conversion by recombinant Salmonella in tumours. *Br. J. Cancer* 89, 1796–1801.

(36) Senanayake, P. K., Kenwright, A. M., Parker, D., and van der Hoorn, S. K. (2007) Responsive fluorinated lanthanide probes for F-19 magnetic resonance spectroscopy. *Chem. Commun.*, 2923–2925.

(37) Takaoka, Y., Kiminami, K., Mizusawa, K., Matsuo, K., Narazaki, M., Matsuda, T., and Hamachi, I. (2011) Systematic Study of Protein Detection Mechanism of Self-Assembling <sup>19</sup>F NMR/MRI Nanoprobes toward Rational Design and Improved Sensitivity. *J. Am. Chem. Soc.* 133, 11725–11731.

(38) Tanaka, K., Kitamura, N., and Chujo, Y. (2011) Bimodal Quantitative Monitoring for Enzymatic Activity with Simultaneous Signal Increases in <sup>19</sup>F NMR and Fluorescence Using Silica

Nanoparticle-Based Molecular Probes. *Bioconjugate Chem.* 22, 1484–1490.

(39) Mizukami, S., Takikawa, R., Sugihara, F., Shirakawa, M., and Kikuchi, K. (2009) Dual-Function Probe to Detect Protease Activity for Fluorescence Measurement and F-19 MRI. *Angew. Chem., Int. Ed.* 48, 3641–3643.

(40) Mizukami, S., Takikawa, R., Sugihara, F., Hori, Y., Tochio, H., Walchli, M., Shirakawa, M., and Kikuchi, K. (2008) Paramagnetic relaxation-based F-19 MRI probe to detect protease activity. *J. Am. Chem. Soc.* 130, 794–5.

(41) Higuchi, M., Iwata, N., Matsuba, Y., Sato, K., Sasamoto, K., and Saido, T. C. (2005) F-19 and H-1 MRI detection of amyloid beta plaques in vivo. *Nat. Neurosci.* 8, 527–533.

(42) Tanabe, K., Harada, H., Narazaki, M., Tanaka, K., Inafuku, K., Komatsu, H., Ito, T., Yamada, H., Chujo, Y., Matsuda, T., Hiraoka, M., and Nishimoto, S. (2009) Monitoring of Biological One-Electron Reduction by F-19 NMR Using Hypoxia Selective Activation of an F-19-Labeled Indolequinone Derivative. *J. Am. Chem. Soc.* 131, 15982–3.